

Development of Simulation Tools for Selective Laser Melting Additive Manufacturing

Thomas Nolan*, Yongsheng Lian*, Mark Sussman†

*Department of Mechanical Engineering, University of Louisville, Louisville, KY

†Department of Mathematics, Florida State University, Tallahassee, FL

Abstract

Two simulation tools have been developed to simulate selective laser melting. One is based on a multiphase flow solver with dynamic mesh adaptation and massive parallelism. The simulation tool is based on a first-principles approach to simulate complex additive manufacturing processes at the entire built part/component level. The developed model takes into account of heating, melting, powder-to-solid volumetric consolidation, cooling, as well as solidification and shrinkage that are often ignored in current simulation tools. The second tool is to solve the heat equation only without considering the flow field and volumetric changes. In both tools laser is modeled as a heat source. The reported work is our first step toward the development of a complete software suite that can be executed rapidly on workstations and clusters with accelerators. The simulation tool can provide AM practitioners and researchers from industry and academic a fast and accurate simulation-based approach to replace current trial-and-error based practices in industry for process and material development.

Introduction

Laser and metal powder based additive manufacturing (AM), specifically Laser sintering (LS) and Direct Digital Manufacturing (DDM), offers design freedom over the constraints of traditional manufacturing methods [1, 2]. LS is a process in which a high-energy laser beam scans a powder bed surface to melt the powder (ceramics, metal, or polymer) to form a bulk part [3]. The most common terminology for LS of metals is Selective Laser Melting (SLM) [4]. SLM can benefit from better design and lower cost, but LS is complicated due to the fast laser scanning rates and complex heat transfer and phase change processes [5-7]. There is a poor understanding of the important physical processes dealing with laser-material interactions, the heat transfer and molten metal flow, and metal phase transformations and thermal stresses, which hinders quality of a finished bulk part, such as density, dimensions, mechanical properties, and microstructure [7, 8]. Previous research also found the temperature field was inhomogeneous [9-13]. And large thermal gradients increase residual stresses and deformation in metals and may lead to crack formation in a bulk part, which leads to the develop of serious problem in the SLM process [14].

Due to the importance of temperature distribution in LS, researchers have grown towards understanding the SLM process [10, 15-19] and creating models to describe the thermal evolution of LS [5, 9, 11, 20-22]. Simulation models can demonstrate the influence of various parameters and are essential tools for identifying the proper parameters without expensive experimental testing.

Various heat transfer processes occur in the SLM. Figure 1 shows the representation of heat transfer in SLM [23]. It consists of radiation at the powder bed, convection between the powder bed and the environment of an air void or gas filled chamber, and heat conduction inside the powder bed and between the bed and substrate. The powder phase change is another important phenomenon in SLM, and phase change can significantly change thermal properties of the powder during SLM.

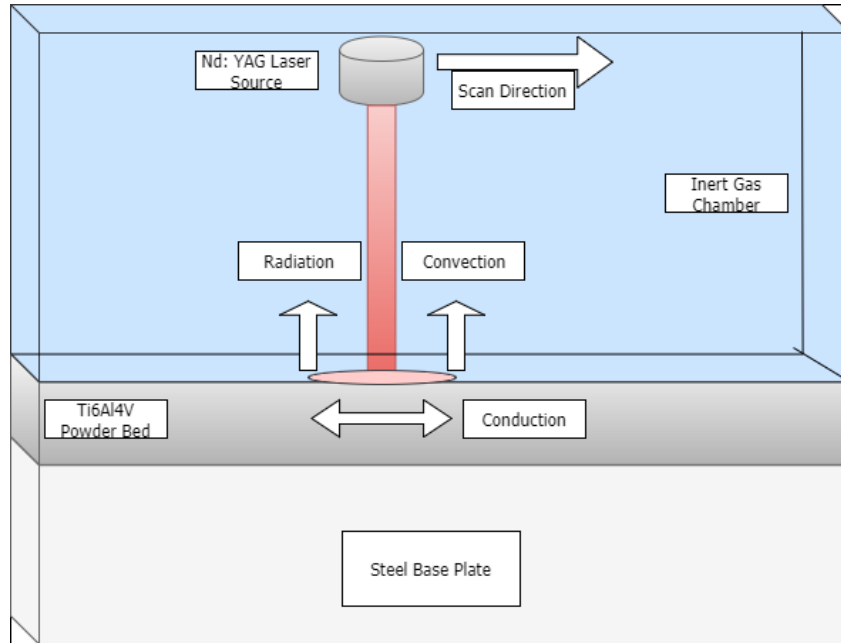


Figure 1. Schematic representation of heat transfer

SLM metal temperature distribution has been modeled with heat equations without considering the flow field [13, 23-29]. Some researchers ignore the heat source as internal energy [30-32], but other studies put the source into the boundary condition equation [5, 20]. Other employ phase change and enthalpy to study the temperature field in SLM [5, 20, 30]. Another model considers influence from metal powder shrinkage and the molten pool fluid flow. Chan and Mazumder showed that fluid flow through the molten pool had a significant effect of the homogeneity of the sintering weld [33]. Some consider that the molten pool influences the thermal field in SLM. The model to simulate melting and solidification has been developed and used by [34-40]. One-dimensional melting in mixed powders has been solved analytically by [37]. A three-dimensional model has been created that considers the thermal behavior and fluid dynamics in the molten pool caused by Marangoni and buoyancy forces along with the melt pool flow caused by gravity and capillary forces [39]. The model also accounts for powder shrinkage due to density and uses a fixed grid temperature transfer model for modeling the melting and solidification of the powder. The model has been compared to the cross-sectional profile for the melt-solid interface in laser processing for nonporous metal experiments. The results show that the thermocapillary force, shrinkage, and buoyancy force dominate the melting and fluid flow [39].

Another thermal evolution of SLM as a heat transfer process utilizes the Fourier heat conduction theory with a Gaussian laser source embedded as an internal energy and the volume-of-fluid method to study the multiphase interaction forces and temperature variation in Ti-6Al-4V powder. Unlike the model from [39], the Marangoni and buoyancy forces are not considered. The latent

heat is dependent on temperature and considers liquid phase of the powder particles. The model uses a volume fraction transport equation to present the distribution of metal and gas phase within the computation domain. The model has been compared to a cross-sectional profile for the distribution of the melting pool.

Various models have been proposed to model the heat transfer from laser beam. Some models have sought to use the volumetric laser beam distribution assumption. Niebling and Otto considered a volumetric line heat source [41]. Gusarov and Yadroitsev used a radiation transfer equation with an isotropic scattering term to describe laser beam penetration [30]. Although the laser beam penetration problem has been studied, Kolossov and Boillat found that with an element size larger than five gradient diameters, the laser beam penetration can be ignored [12]. Realizing the interaction between the laser beam and powder bed, leads to a greater understanding of laser beam penetration and absorption. Several models consider the absorption a constant ratio for the bulk powder [20, 42-46]. Laser beam absorption in powder depends on several factors including oxidation level, surface type, surface temperature, and laser beam wavelength. In the case of metal powders, the laser beam absorption ratio varies within a few percent of the molten absorption ratio [47].

Thermal properties of metal powder include density, enthalpy, heat capacity, and thermal conductivity. Carslaw and Jaeger show that thermal conductivity varies with temperature [48]. SLM uses an effective thermal conductivity. It has also been shown that the porosity of the powder bed influences thermal conductivity. The effective thermal conductivity is a function of the thermal conductivities of solid metal and gas in the powder voids [3, 20, 49].

The main consideration of thermal conductivity of metal powders is the temperature near the melting point and above in liquid state. Without experimental data, a constant thermal conductivity is assumed. Thummler proposed that thermal conductivity is influenced by powder porosity and pore geometries and thermal conductivity is controlled by gas content in the voids of the powder [50]. Rombouts et al. showed that thermal conductivity is independent of powder material and depends on porosity and size of voids in the powder along with depending on gas content in the voids [51]. Roberts and Wang show that the thermal conductivity of Ti6Al4V powder is low for powder and increases dramatically when nearing the melting point [20]. The density and heat capacity of metal powder is shown as the mass average of each state's (powder, liquid, solid) value [49]. Some consider the heat capacity to be separate at each phase and use an effective heat capacity that is temperature dependent [46].

In this paper, we present two models to study SLM. One is based on commercial software Fluent, and the other one is based on an in house multiphase flow solver. In the first approach, we solve the heat transfer equations without considering the flow field. The laser is modeled as a three-dimensional Gaussian energy source that is imposed on a two-dimensional surface. This approach only considers the heat transfer without the phase change. In the second approach, we will model the phase change using multiphase flow solver.

Numerical Models

In the following we introduce the two models used to study SLM. The first one is based on a simple heat equation (the heat conduction model) and the second one is based on a multiphase flow solver (multiphase flow model).

Heat Conduction Model

The most common thermal evolution of SLM as a heat transfer process can be described by Fourier heat conduction theory. Equation (1) describes the governing heat conduction in a moving medium [48],

$$\lambda \left(\frac{\partial^2 T}{\partial x^2} + \frac{\partial^2 T}{\partial y^2} + \frac{\partial^2 T}{\partial z^2} \right) + q = \rho c \frac{\partial T}{\partial t} \quad (1)$$

The initial condition and boundary conditions are as follows:

$$\text{Initial temperature:} \quad T(x, y, z, 0) = T_0 \quad (2)$$

$$\text{Surface convection and radiation:} \quad -\lambda \frac{\partial T}{\partial z} = \varepsilon_\theta \sigma (T^4 - T_e^4) + h(T - T_e) \quad (3)$$

$$\text{No heat loss at the bottom:} \quad -\lambda \frac{\partial T}{\partial z} \Big|_{z=0} = 0 \quad (4)$$

where T is the temperature, λ the conductivity coefficient, ρ is the density, c is the heat capacity coefficient, q is the internal heat, T_0 is the powder bed initial temperature, T_e the environment temperature, ε_θ the thermal radiation coefficient, σ the Stefan-Boltzmann constant, and h the convection heat transfer coefficient. The governing equations were used to study the thermal field of dental porcelain in SLM [47].

Multiphase Flow Model

The second approach is based on a multiphase flow solver. In this approach the governing equations to be solved are the three-dimensional Navier-Stokes equations for immiscible, multiphase flows, which are given as follows:

$$\nabla \cdot \vec{V} = 0 \quad (5)$$

$$\rho \left(\frac{\partial \vec{V}}{\partial t} + \vec{V} \cdot \nabla \vec{V} \right) = -\nabla p + \nabla \cdot \left(\mu \left(\nabla \vec{V} + (\nabla \vec{V})^T \right) \right) + F_{tension} + \rho \vec{g} \quad (6)$$

$$\rho c_v \left(\frac{\partial T}{\partial t} + \vec{V} \cdot \nabla T \right) = -\nabla \cdot \vec{q} \quad (7)$$

where $\vec{V} = (u, v, w)$ is the velocity vector, ρ is the density, t is the time, p is the pressure, μ is the viscosity, \vec{g} is the gravitational acceleration vector, \vec{q} is the heat flux vector.

Besides the above temperature condition at the interface, the following mass conservation must be satisfied across the interface [52]

$$\dot{m} = \rho_L (\vec{V}_I \cdot \vec{n} - V_L \cdot \vec{n}) = \rho_s (\vec{V}_I \cdot \vec{n} - V_s \cdot \vec{n}) \quad (8)$$

where \dot{m} is the interfacial mass flux, ρ_L and ρ_s are the densities of liquid and solid phases respectively, \vec{n} is the normal pointing from solid to liquid, $\vec{V} \cdot \vec{n}$ is the normal velocity of the fluid, and $\vec{V}_I \cdot \vec{n}$ is the normal velocity of the interface. The energy conservation at the interface equation satisfies the Rankine-Hugoniot jump condition

$$\dot{m}(h_L - h_s) = \vec{q}_L \cdot \vec{n} - \vec{q}_s \cdot \vec{n} \quad (9)$$

where h_L and h_s are the enthalpy of the liquid and solid phases respectively.

The liquid-solid interface can be represented by a zero level set of a distance function. The distance equation is given by the following equation [52]

$$\frac{\partial \phi}{\partial t} + \vec{V} \cdot \nabla \phi + \frac{\dot{m}}{\rho_L} |\nabla \phi| = 0 \quad \text{or} \quad \frac{D\phi}{Dt} + \frac{\dot{m}}{\rho_L} |\nabla \phi| = 0 \quad (10)$$

where ϕ is the distance to the piecewise linear moment of fluid reconstructed interface. The multiphase flow solver solves the three-dimensional Navier-Stokes equations using the variable density pressure projection algorithm [53] on block structured adaptive mesh refinement grid (AMR) [54]. It can handle both compressible [55] and incompressible flows [56, 57]. The solver employs the state of the art moment of fluid method (MOF) [58-60] to represent multiphase interfaces [55, 61-64]. It employs dynamic contact models for droplet impact problems [65]. Our tests show that the code has a high parallel efficiency of more than 96% on a 48-core workstation.

Interface representation

During the MOF interface reconstruction process, a reference volume fraction function F_{ref} and a reference centroid, \mathbf{x}_{ref}^c , both corresponding to the real interface, are given [Figure 2a], and the actual volume fraction function, F_A , and the actual centroid, \mathbf{x}_A^c , corresponding to the reconstructed interface, are then computed [Figure 2b].

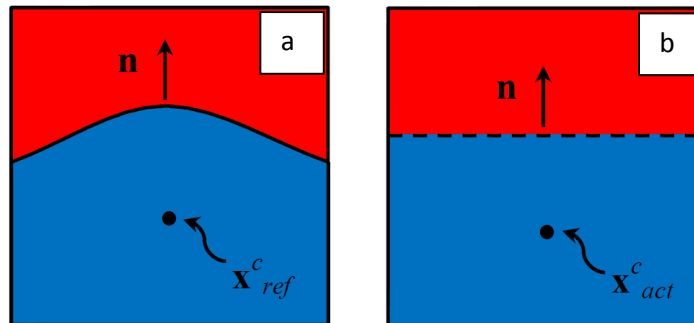


Figure 2. Surface reconstruction using the MOF method [56]. (a) the real interface and reference volume fraction and centroid; (b) the reconstructed interface and computed volume fraction and

centroid. The MOF reconstruction requires the reconstructed volume to be equal to the reference volume while the reconstructed centroid as close to the reference centroid as possible.

The MOF method requires that the actual volume fraction be equal to the reference value and the actual centroid be as close to the reference centroid as possible. This becomes a constraint optimization problem formulated as follows:

$$\text{Minimize} \quad \left\| \mathbf{x}_{ref}^c - \mathbf{x}_A^c(\mathbf{n}, b) \right\|^2 \quad \text{under constrain:} \quad \left| F_{ref} - F_A(\mathbf{n}, b) \right| = 0 \quad (11)$$

As discussed in [57], the use of centroid information ensures the MOF method maintains a sharp interface which is critical for the droplet impact simulation because the thickness of the lamella is about two orders of magnitude smaller than the initial droplet diameter [66].

In our numerical models, we used two different materials to differentiate the liquid drop and the liquid film to illustrate the pertinent fluid dynamics features in the drop impact on thin film. The method is illustrated in Figure 3. We first reconstruct the interface for the material whose centroid is furthest the centroid of the computational cell by solving Eq. (13). In the case shown in Figure 3 it is the red material. Next, we reconstruct the interface for the remaining material whose centroid is furthest to the centroid of the unoccupied region in the cell (white region) by solving Eq. (13). In Figure 3 the next material is marked in blue. This procedure continues until all the material interfaces are constructed.

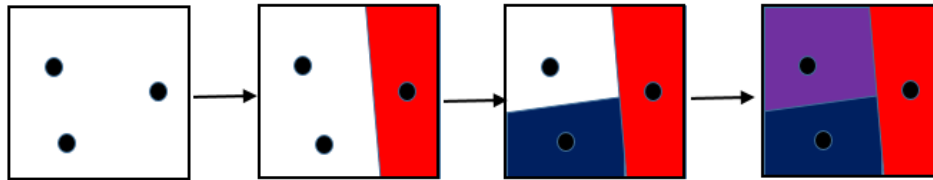


Figure 3. MOF interface reconstruction with three materials in one cell

Adaptive mesh refinement

The Navier-Stokes equations are solved using the variable density pressure projection algorithm [53] on the block structured adaptive mesh refinement grids [54, 67]. The grid adaption is based on the triple point region and the curvature of the interface. As shown in Figure 4, the grid refinement is performed near regions where curvature is greater than a predefined value. The adaptive mesh refinement method ensures fine grid is only used in the regions of interests, which maintains the accuracy of the solver at reasonable computational cost.

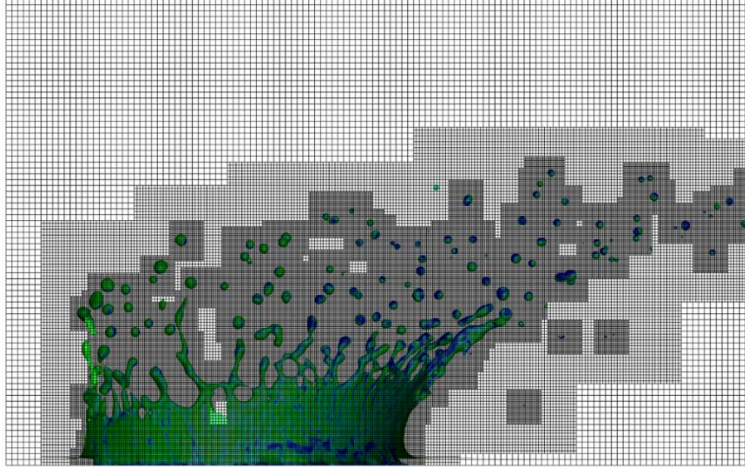


Figure 4. Two-level adaptive mesh refinement

Laser Source Term Model

The modeling of laser beam characteristics has been researched to better understand the LS process. Simple models assume the laser beam to be a point source, but this conjecture is not representative of reality. It has been shown that laser beam sources can be characterized by three parameters: diameter, power, and intensity distribution. Courtney and Steen deduced an effective Gaussian beam diameter equivalent using measurements from a laser beam and comparing to a Gaussian laser beam diameter [68]. This effective Gaussian laser beam diameter is the most widely used for simulation [20]. In this model the laser intensity distribution can be written as

$$I(r) = I_0 e^{(-d^2/d_1^2)} \quad (12)$$

where d_1 is the beam diameter, I_0 is the irradiance that diminishes exponentially, and d is the radius of a point from the center of the laser beam source. The thermal heat flux distribution is

$$q(r) = \frac{2P}{\pi r_0^2} e^{-\frac{2r^2}{r_0^2}} \quad (13)$$

where P is the laser power, r_0 is the spot radius, and r is the radial distance. The total heat flux on a circular surface of radius r_0 can be calculated by integrating the heat flux

$$q_m = \frac{\alpha}{\pi r_0^2} \int_0^{r_0} q(2\pi r) dr = \frac{0.865\alpha P}{\pi r_0^2} \quad (14)$$

where α is absorption rate.

The laser beam distribution is typically assumed to be either surface or volumetric. The surface variation of the laser beam is the most common because of the lack of research into laser beam penetration in the volumetric distribution [9, 30, 69]. In an attempt to solve the lack of understanding of the volumetric distribution, Wang and Laoui used a ray tracing (RC) model that predicts the absorption and reflection of laser beam energy on each particle produced by a large

number of rays [9]. The energy absorbed by each particle is totaled and the total energy delivered by the laser is totaled. From the total energy calculation energy, penetration can be described as a depth function into the powder.

Li et al. used the assumption that the laser beam distribution is surface in nature, but also includes the convection and radiation terms from the Fourier heat conduction theory [46]. The laser source model is

$$S_{laser}(x) = \left[\alpha \frac{P}{\pi r_0^2} \exp \left[-\frac{2(x - vt - x_i)^2}{r_0^2} \right] - \varepsilon_\theta \sigma (T^4 - T_e^4) + h(T - T_e) \right] \delta \quad (15)$$

where α is the absorptivity, P is laser power, r_0 is the laser beam radius, v is scanning velocity, x is the laser beam position, x_i is the initial laser beam position, ε_θ is the black body radiation, σ is Boltzmann's constant, T is melt pool temperature, T_e^4 is environment temperature, and δ is a delta function. The purpose of the laser source equation is to mark the position of the powder particle surface in the flow field. The laser source is implemented at the beginning of simulation until end of the laser beam path.

Numerical Results

The model represents IN718 powder on top of a steel plate with air surroundings. The process parameters and thermal properties are taken from [46] and [70]. Table 1 shows the model and process parameters. ANSYS Fluent is used to create the simulation. The laser beam is modeled as Gaussian distribution with a 100 μm laser spot size. The element size is 100 μm in a 0.8 cm by 0.4 cm by 0.226 cm computation domain and 73600 elements. The laser scans from left to right. Convection and radiation are modeled using a mixed heat transfer coefficient at the powder surface included in the source term. The initial temperature is set at 300 K. The density and thermal conductivity are functions of temperature. The specific heat is constant.

The model is set up using a rectangular solid Ti6Al4V part with mesh and a user defined laser beam source beam function taken from [46]. The laser source is implemented at the start of the simulation and continues until the laser beam moves over the entire path of the domain.

The mesh is shown in Figure 5. The temperature profile for the first layer scan is shown in Figure 6., and Figure 7.. The temperature distribution contours show an ellipse-like shape that repeats as the profile moves from the center, which is shown in [71]. The melt pool moves linearly maintaining the ellipsoid shape throughout. The melt pool also maintains a similar shape and temperature concentration at each time instant. The plots also show the concentration of the thermal gradient at the front of the molten pool, which is due the movement of the laser beam source and the temperature and phase dependent material properties.

Figure 8 shows a comparison of the experimental results to our simulation. The center and shape of the temperature field in our simulation are like those of the experimental results. The temperatures also reach similar values to the experiment.

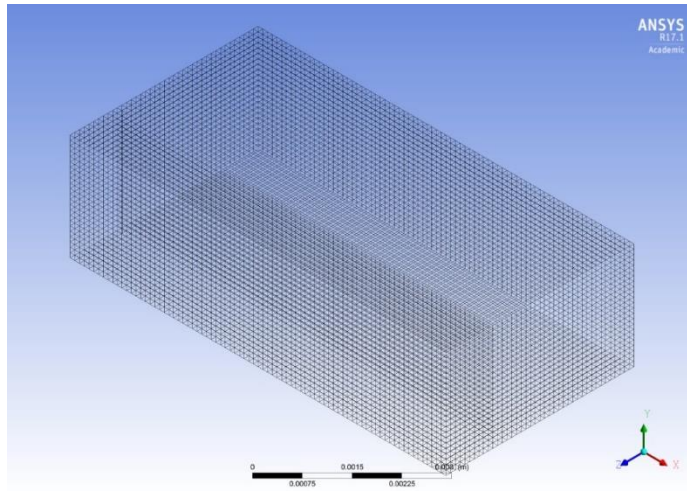


Figure 5. Simulation Mesh

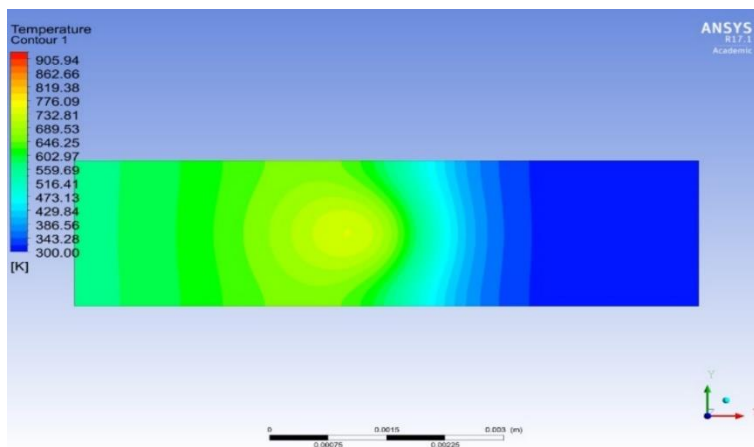


Figure 6. Temperature gradient profile at 0.394 s

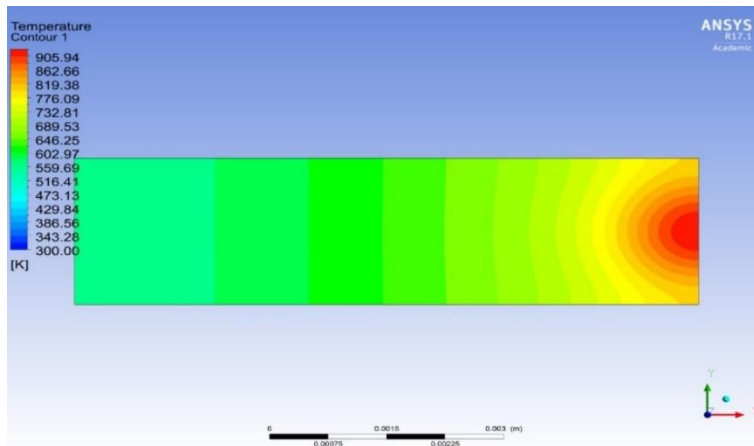


Figure 7. Temperature gradient profile at 0.787 s

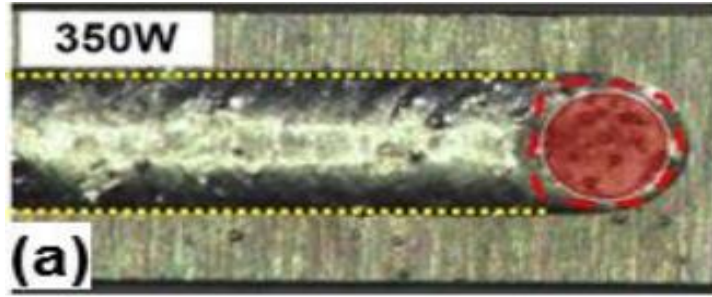


Figure 8. Temperature gradient profile compared to experiment

| Nomenclature | Symbol | Value |
|--|-------------------|---|
| Laser Power (W) | P | 350 |
| Laser Distribution | | Gaussian |
| Laser beam radius (m) | r_0 | 5×10^{-5} |
| Scanning Speed (cm/s) | v | 1.016 |
| Surrounding temperature (K) | T_∞ | 300 |
| Absorption | α | 0.35 |
| Density of Ti6Al4V (g/cm^3) | ρ | $8.19-39.2\text{E-}2*(\text{T}-298)$ |
| Mixed Heat Transfer coefficient ($\text{W/m}^2\text{k}$) | h | 10 |
| Specific Heat of IN708 (j/g-K) | C_p | 0.65 |
| Thermal conductivity of Ti6Al4V (W/m-K) | k | $39.73+32.4\text{E-}3*\text{T}+2\text{E-}5\text{T}^2$ |
| Black body radiation | ϵ_θ | 1 |
| Boltzmann's constant | σ | 5.67×10^{-8} |
| Model size (cm) | | $0.8 \times 0.4 \times 0.226$ |

Table 1. Model and process parameters

In Figure 9 we show the simulated melting process using our proposed multiphase flow solver. Three metal particle of the same radii of $30 \mu\text{m}$ are put side by side. The laser source model of Eq. (15) is used. The laser power is 175 W and scan speed is 1.25 m/s. The density and thermal conductivity of the Ti6Al4V are assumed to be constant. The melting process is captured by the solver. Our simulation also shows that the particle is not fully melted.

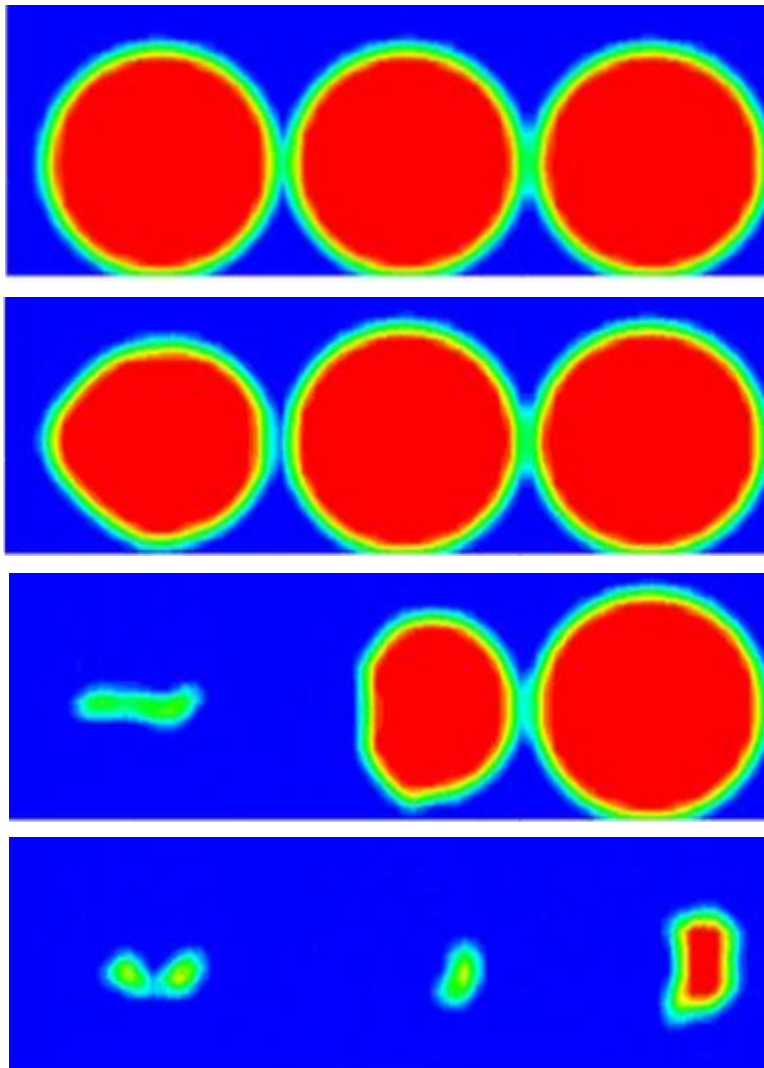


Figure 9. Simulated melting process based on the multiphase flow solver. (Red: Solid Ti6A14V).

Conclusions

We presented two models to study SLM. The first model is based on the simple heat conduction equation that considers the heat transfer but not the flow field or volumetric changes. The other model is based on a multiphase flow solver that considers the heat transfer, phase change and volumetric changes.

Acknowledgement

This work is partially supported by a NASA Grant.

References

1. Zhong, M. and W. Liu, *Laser surface cladding: The state of the art and challenges*. Journal of Mechanical Engineering Science, 2010. **224**(C5): p. 1041-1060.
2. Zhou, J.H., Y.W. Zhang, and J.K. Chen, *Numerical simulation of random packing of spherical particles for powder-based additive manufacturing*. Journal of Manufacturing Science and Engineering: ASME, 2009. **131**(3).
3. Cervera, G.B.M., *Numerical prediction of temperature and density distributions in selective laser sintering processes*. Rapid Prototyping Journal, 1999. **5**(1): p. pp.
4. Gibson, L., D. Rosen, and B. Stucker, *Additive manufacturing technologies: rapid prototyping to direct digital manufacturing*. 2009, New York, NY: Springer.
5. Tolochko, N.K., *Mechanisms of selective laser sintering and heat transfer in Ti powder*". Rapid Prototyping Journal, 2003. **9**(5): p. 314-326.
6. Harris, I.D. and A. Director, *Development and implementation of metals additive manufacturing*. 2011, DOT International, New Orleans.
7. Frazier, W.E., *Metal additive manufacturing: A review*. Journal of Materials Engineering and Performance, 2014. **23**(6): p. 1917-1928.
8. Bordia, R., S. Kang, and E. Olevsky, *Current understanding and future research directions at the onset of the next century of sintering science and technology*. , Journal of the American Ceramic Society.
9. Wang, X.C. and T. Laoui, *Direct Selective Laser Sintering of Hard Metal Powders: Experimental Study and Simulation*. Int J Adv Manuf Technol, 2002. **19**: p. 351-357.
10. Kruth, J.P. and X. Wang, *Lasers and materials in selective laser sintering*. Assembly Automation, 2003. **23**(4): p. 357-371.
11. Simchi, A., *Direct laser sintering of metal powders: Mechanism, kinetics and microstructural features*. Materials Science and Engineering: A, 2006. **428**(1): p. 148-158.
12. Kolossov, S. and E. Boillat, *3D FE simulation for temperature evolution in the selective laser sintering process*. International Journal of Machine Tools and Manufacture, 2004. **44**: p. 2-3.
13. Zhang, D.Q. and Q.Z. Cai, *Select laser melting of W-Ni-Fe powders: simulation and experimental study*. The International Journal of Advanced Manufacturing Technology, 2010. **51**(5): p. 649-658.
14. Contuzzi, N. and S.L. Campanelli, *"3d Finite element analysis in the selective laser melting process"*, Int j simul. model, 2011. **10**(3): p. 113-121.
15. Kruth, J.P. and G. Levy, *Consolidation phenomena in laser and powder-bed based layered manufacturing*. CIRP Annals - Manufacturing Technology, 2007. **56**(2): p. 730-759.
16. Levy, G.N. and R. Schindel, *Rapid Manufacturing and Rapid Tooling with Layer Manufacturing (Lm) Technologies, State of the Art and Future Perspectives*. CIRP Annals - Manufacturing Technology ,Vol.52, 2003. **2**: p. 589-609.
17. Miani, F., *"Recent Developments Of Direct Metal Selective Laser Sintering"*, available at. 2012.
18. Kruth, J.P. and B. Vandenbroucke, *Benchmarking Of Different Sls/Slm Processes As Rapid Manufacturing Techniques*, in Int. Conf. Polymers & Moulds Innovations (PMI). 2005: Gent, Belgium.
19. Kumar, S., *"Selective Laser Sintering: A Qualitative and Objective Approach"*. JOM Journal of the Minerals, 2003. **55**: p. 10-43.
20. Roberts, I.A. and C.J. Wang, *A three-dimensional finite element analysis of the temperature field during laser melting of metal powders in additive layer manufacturing*. International Journal of Machine Tools and Manufacture, 2009. **49**(12): p. 916-923.

21. Fischer, P. and V. Romano, *Sintering of commercially pure titanium powder with a Nd:YAG laser source*. Acta Materialia, 2003. **51**(6): p. 1651-1662.
22. Singh, S. and D. Roy, *Studies on laser sintering of mechanically alloyed Al50Ti40Si10 composite*. Materials Science and Engineering, Vol.501, 2009. **1**: p. 242-247.
23. Li, Y. and G. Dongdong, *Parametric analysis of thermal behavior during selective laser melting additive manufacturing of aluminum alloy powder*. Materials & Design, 2014. **63**: p. 856-867.
24. Jianguai, L. and S. Yusheng, *Numerical Simulation of Transient "Temperature Field in Selective Laser Melting"*. China Mechanical Engineering, Vol, 2008. **19**(20): p. 2492-2495.
25. Wei Jiang, K.W.D. *"Finite Element Analysis of Residual Stresses"*. 2012.
26. Zhao, B. and H. Shi, *"Modeling of Selective Laser Sintering for PC Powder"*. Journal of Beijing University of Aeronautics and Astronautics, 2002. **28**(6): p. 660-663.
27. Yifu, S. and G. Dongdong, *Simulation of Temperature Field in Direct Metal Laser Sintering Processes*. China Mechanical Engineering, Vol.16, 2005. **1**: p. 67-73.
28. Jian, X. and S. Xiaogang, *Simulation and testing of the transient temperature field of infrared laser sintering*. Acta Photonica Sinica, 2011. **32**(7): p. 965-968.
29. Jian, X. and S. Xiaogang, *Simulation and testing of the transient temperature field of infrared laser sintering*. Acta Photonica Sinica, 2009. **38**(6): p. 1327-1330.
30. Gusarov, A.V. and I. Yadroitsev, *Heat transfer modelling and stability analysis of selective laser melting*. Applied Surface Science, 2007. **254**(4): p. 975-979.
31. Li, C. and Y. Wang, *Three-dimensional finite element analysis of temperatures and stresses in wide-band laser surface melting processing*. Materials & Design, 2010. **31**(7): p. 3366-3373.
32. Shuai, C. and P. Feng, *Simulation of dynamic temperature field during selective laser sintering of ceramic powder*. Mathematical and Computer Modelling of Dynamical Systems, Vol.1, 2012. **11**.
33. Chan, C. and J. Mazumder, *A two-dimensional Transient model for convection in laser melting pool*. Metallurgical Transactions. **A**, **15**: p. 1984-2175.
34. Chen, T. and Y. Zhang, *Modeling of laser sintering of two-component metal powder on top of sintered layers via multi-line scanning*. Applied Physics A, 2006. **86**: p. 2-213.
35. Xiao, B. and Y. Zhang, *Laser sintering of metal powders on top of sintered layers under multiple-line laser scanning*. Journal of Physics D: Applied Physics, 2007. **40**(21): p. 6725-6734.
36. Chen, T. and Y. Zhang, *Numerical Simulation of Two-Dimensional Melting and Resolidification of a Two-Component Metal Powder Layer in Selective Laser Sintering Process*, in *Numerical Heat Transfer, Part A: Applications*. 2004. p. 633-649.
37. Zhang, Y. and A. Faghri, *Melting of a subcooled mixed powder bed with constant heat flux heating*. International Journal of Heat and Mass Transfer, 1999. **42**: p. 775-788.
38. Zhang, Y. and A. Faghri, *Three-Dimensional Sintering of Two-Component Metal Powders With Stationary and Moving Laser Beams*. Transactions of the ASME, 2000. **122**: p. 150-158.
39. Xiao, B. and Y. Zhang, *Marangoni and Buoyancy Effects on Direct Metal Laser Sintering with a Moving Laser Beam*, in *Numerical Heat Transfer, Part A: Applications*. 2007. p. 715-733.
40. Konrad, C. and Y. Zhang, *Analysis of melting and resolidification in a two-component metal powder bed subjected to temporal Gaussian heat flux*. International Journal of Heat and Mass Transfer, 2005. **48**(19-20): p. 3932-3944.
41. Niebling, F. and A. Otto, *Analyzing The Dmls-Process By A Macroscopic Fe-Model*.
42. Labudovic, M., *"A three dimensional model for direct laser metal powder deposition and rapid prototyping"*. Journal Of Materials Science, Vol, 2003. **38**: p. 35-49.
43. M. Shiomi, A.Y., *Finite element analysis of melting and solidifying processes in laser rapid prototyping of metallic powders*, in *International Journal of Machine Tools & Manufacture*, Vol.39. p. 237-252.

44. Zhang Jian, L.D.e.a. "*Simulation of Temperature Field in Selective Laser Sintering of Copper Powder*".
45. Song, S.D.B., *Process parameter selection for selective laser melting of Ti6Al4V based on temperature distribution simulation and experimental sintering*. The International Journal of Advanced Manufacturing Technology, 2011. **61**(9-12): p. 967-974.
46. Li, C.J., T.W. Tsai, and C.C. Tseng, *Numerical simulation of heat and mass transfer during selective laser melting of titanium alloys powder*. Physics Procedia, 2016. **83**: p. 1444-1449.
47. Dai, K. and L. Shaw, *Finite element analysis of the effect of volume shrinkage during laser densification*. Acta Materialia, 2005. **53**(18): p. 4743-4754.
48. Carslaw, H.S. and J.C. Jaeger, "*Conduction of Heat in Solids*". 1959: Oxford University Press, Amen House, London E.C.4.
49. J. C. Nelson, N.K.V. "*Laser Sintering Model for Composite Materials*".
50. F. Thummler, R.O., *An Introduction to Powder Metallurgy*. 1993, Cambridge, London: The University Press.
51. Rombouts, M.e.a., *Light extinction in metallic powder beds: correlation with powder structure*. Journal of Applied Physics. **98**(1).
52. Gibou, F., et al., *A level set based sharp interface method for the multiphase incompressible Navier–Stokes equations with phase change*. Journal of Computational Physics, 2007. **222**(2): p. 536-555.
53. Kwatra, N., et al., *A method for avoiding the acoustic time step restriction in compressible flow*. Journal of Computational Physics, 2009. **228**(11): p. 4146-4161.
54. Sussman, M., et al., *An adaptive level set approach for incompressible two-phase flows*. Journal of Computational Physics, 1999. **148**(1): p. 81-124.
55. Jemison, M., M. Sussman, and M. Arienti, *Compressible, Multiphase Semi-Implicit Method with Moment of Fluid Interface Representation*. Submitted to Journal of Computational Physics, 2013.
56. Li, G., Y.S. Lian, and M. Sussman, *Simulations of Gas-liquid Two-phase Jet Flows Using the Moment of Fluid Method*, in *ASME 2013 Fluid Engineering Division Summer Meeting*. 2013.
57. Jemison, M., et al., *A Coupled Level Set-Moment of Fluid Method for Incompressible Two-Phase Flows*. Journal of Scientific Computing, 2012: p. 1-38.
58. Hirt, C.W. and B.D. Nichols, *Volume of fluid (VOF) method for the dynamics of free boundaries*. Journal of computational physics, 1981. **39**(1): p. 201-225.
59. Brackbill, J., D.B. Kothe, and C. Zemach, *A continuum method for modeling surface tension*. Journal of computational physics, 1992. **100**(2): p. 335-354.
60. Pilliod Jr, J.E. and E.G. Puckett, *Second-order accurate volume-of-fluid algorithms for tracking material interfaces*. Journal of Computational Physics, 2004. **199**(2): p. 465-502.
61. Lian, Y.S., Y.S. Guo, and A. Work, *Study of supercooled large droplet impacts using the moment of fluid method*, in *52nd AIAA Aerospace Sciences Meeting*. 2014.
62. Dyadechko, V. and M. Shashkov, *Moment-of-fluid interface reconstruction*. Los Alamos report LA-UR-05-7571, 2005.
63. Arienti, M., et al., *Coupled level-set/volume-of-fluid method for simulation of injector atomization*. Journal of Propulsion and Power, 2012. **29**(1): p. 147-157.
64. Arienti, M. and M. Sussman, *An embedded level set method for sharp-interface multiphase simulations of Diesel injectors*. International Journal of Multiphase Flow, 2014. **59**: p. 1-14.
65. Lian, Y.S., et al. *Multiphase flow simulation using moment of fluid method*. in *The 8th International Conference on Computational Fluid Dynamics*. 2014. Chengdu, Sichuan, P.R. China.
66. Šikalo, Š., et al., *Dynamic contact angle of spreading droplets: Experiments and simulations*. Physics of Fluids, 2005. **17**: p. 062103.

67. Sussman, M., *A parallelized, adaptive algorithm for multiphase flows in general geometries*. Computers & Structures, 2005. **83**(6-7): p. 435-444.
68. Courtney, C. and W.M. Steen, *Measurement of the diameter of a laser beam*. Applied physics, 1978. **17**(3): p. 303-307.
69. Gusarov, A.V. and J.P. Kruth, *Modelling of radiation transfer in metallic powders at laser treatment*. International Journal of Heat and Mass Transfer, 2005. **48**(16): p. 3423-3434.
70. Juan J. Valencia, P.N.Q., *Thermophysical Properties*. ASM, 2008. **15**: p. 468-481.
71. Zhang, D.Q. and Q.Z. Cai, *Select laser melting of W–Ni–Fe powders: simulation and experimental study*. The International Journal of Advanced Manufacturing Technology, 2010. **51**: p. 5-8.